Dynamic Improvement and Efficiency Optimization of Wireless Power Transfer Systems Using Improved FCS-MPC and P&O Methods

Shuo Chen, *Student Member, IEEE*, Wen Ding, *Member, IEEE*, Lujie Huo, *Student Member, IEEE*,
Xiang Wu, *Member, IEEE*, Shuai Shi, and Ruiming Hu

***Abstract*—This article proposes a novel control scheme using finite-control-set model predictive control (FCS-MPC) and perturbation and observation (P&O) method for the dynamic improvement and efficiency optimization of dual-side *LCL* compensated wireless power transfer systems. First, the rectifier at the secondary side incorporates the proposed FCS-MPC with adaptive step-size and improved cost function to achieve the fast response of output voltage. The linear extended state observer is designed to combine with FCS-MPC to avoid using extra current sensors. The two-stage series prediction method is proposed to reduce the computational burden. Meanwhile, on the premise of ensuring the stability of output voltage, the inverter at the primary side is controlled by the adaptive P&O method for maximum energy efficiency tracking (MEET) by minimizing the input dc current. Different system stages, i.e., tracking stage and oscillation stage, for MEET are defined and distinguished. The adaptive perturbation step-size is designed according to different system stages so as to remove the tradeoff between the oscillation and convergence rate in the conventional method. Finally, the effectiveness of the cooperative control of FCS-MPC and adaptive P&O method is verified by experimental results.**

***Index Terms*—Dynamic improvement, finite-control-set model predictive control (FCS-MPC), maximum energy efficiency tracking (MEET), perturbation and observation (P&O), wireless power transfer (WPT).**

NOMENCLATURE

f_s	Resonant frequency of compensation networks.
P_{in}, P_{out}	System input and output power.
V_{in}, V_{out}	DC input and output voltages.
I_{in}, I_{out}	DC input and output currents.
L_{pt}, L_{st}	Self-inductances of dual-side coils.
L_{pi}, L_{si}, C_{pt}, C_{st}	Compensation networks' components.
M	Mutual inductance of dual-side coils.
k	Coupling coefficient.
C_f	Filtering capacitor for system output.
R_L	Load resistance.
V_{pi}, V_{si}	Dual side converters' output voltages.
φ_p, φ_s, θ	Phase shift angles of primary and secondary sides.
P_{out}, Q_{out}	Active and reactive output power.
η	System efficiency.
P_{res}	Resistance loss of resonant networks.
P_{inv}	Inverter loss.
P_{rec}	Rectifier loss.
I_{siRMS}	RMS value of I_{si}.
β_1, β_2	Adjustable gains of linear ESO.
ω_n	Bandwidth of linear ESO.
Δf	Finest phase shift value in the digital controller.
f_c	Clock frequency of digital controller.
n	Number of elements of finite control set.
J_1	Cost function of the first prediction.
J_2	Cost function of the second prediction.
Δ_{adp}	Adaptive step-size of FCS-MPC.
V_m	Saturation voltage error.
λ	Gain of voltage error.
α	Weighting factor in cost function.
sum	Sum of *N* in *t* number of consecutive periods.
Δ_{const}	Constant perturbation step-size.
Δ_{step}	Variation of perturbation step-size.
$\Delta_{\min}$	Minimum perturbation step-size.
Δ_{PO}	Adaptive perturbation step-size.
I_r	Variation rate of input dc current.
I_{thr}	Threshold of variation rate of input dc current.
T_p	Voltage control period.
T_r	Control period of P&O method.

I. INTRODUCTION

WIRELESS power transfer (WPT) based on magnetic resonance achieves the power transmission over an air-gap through weak magnetic coupling without physical connections,

Manuscript received 20 March 2023; revised 9 June 2023 and 11 July 2023; accepted 2 August 2023. Date of publication 7 August 2023; date of current version 22 September 2023. This work was supported by the National Natural Science Foundation of China under Grant 52077164. Recommended for publication by Associate Editor A. Barrado. *(Corresponding author: Wen Ding.)*

Shuo Chen, Wen Ding, Lujie Huo, Shuai Shi, and Ruiming Hu are with the School of Electrical Engineering, Xi'an Jiaotong University, Xi'an 710049, China (e-mail: ts17130047a3@cumt.edu.cn; wending@mail.xjtu.edu.cn; 3122304053@stu.xjtu.edu.cn; 3120304037@stu.xjtu.edu.cn; huruiming@stu.xjtu.edu.cn).

Xiang Wu is with the School of Electrical and Power Engineering, China University of Mining and Technology, Xuzhou 221008, China (e-mail: cumtwuxiang@cumt.edu.cn).

Color versions of one or more figures in this article are available at https://doi.org/10.1109/TPEL.2023.3302614.

Digital Object Identifier 10.1109/TPEL.2023.3302614

which was proposed by Nikola Tesla more than 100 years ago [1]. Over several decades, WPT system has been continuously developed because of its safety, convenience, high robustness and reliability, and long product lifespan [2]. Until recently, it has been attracting the scholars' attentions and extensively applied in the fields of electrical vehicles [3], [4], [5], bio-medical implants [6], portable electronic devices [7], underwater equipment [8], wireless motor [9], [10], and even train [11], which has the power level ranging from milliwatt to megawatt.

Efficiency has always been one of the most important indicators to evaluate WPT systems. In [12], the concept of "maximum energy efficiency tracking (MEET)" is strictly distinguished from "maximum power transfer tracking." But the efficiency of WPT system changes with many factors, such as the coupling coefficient, the load condition, and the quality factor. It is a key research topic that how to improve the system efficiency. Many methods focused on this topic have been published, which are roughly fallen into frequency shifting method, passive component tuning method, and equivalent impedance matching method. Frequency shifting method achieves the efficiency optimization by regulating the switching frequency of inverter [13]. However, because the switching frequency of inverter is far away from the resonant frequency, the reactive power is large and the system efficiency is relatively low. For the passive component tuning method, the MEET for WPT systems is attained by adjusting the inductance or capacitance values dynamically. In [14], dual switch-controlled capacitors are introduced in the series–series (S-S) compensated WPT system to realize the impedance-matching for efficiency optimization. Li et al. [15] adopt the auxiliary variable inductor for the S-S compensated WPT system to achieve the high system efficiency. However, the extra passive component and control circuit could increase the loss, cost, and volume of the system, which limits the practical application of this method. The equivalent impedance matching method is implemented by controlling the dc–dc converters or active rectifiers for the goal of efficiency optimization. In [16], two buck–boost converters are adopted in primary and secondary sides to realize the constant voltage (CV) output and efficiency optimization. In [17], a buck converter is added in the primary side to facilitate the implementation of impedance matching. Nevertheless, the extra dc–dc converters also increase the loss, cost, and size of the system. Active rectifiers combined with phase shift control (PSC) can be used to achieve the constant output and maximum efficiency tracking without the extra dc–dc converters. Dual PSC [18], triple PSC [19], and even quadra-variable control [20] are proposed to regulate output and optimize efficiency for WPT systems with dual-side full-bridge converters. However, the track of maximum efficiency point in these methods is based on the ideal passive components and the ignored converter losses, which may deviate from the actual maximum efficiency point. In [21], the mode switching of dual full-bridge converters between full-bridge and half-bridge is presented to realize the semi-impedance-matching for the efficiency improvement. This method is simple and effective, but the maximum efficiency point cannot be tracked. In [22], the perturbation and observation (P&O) method is first adopted to track the maximum energy efficiency for WPT system by minimizing the dc input power. Similarly, P&O methods for tracking the maximum energy efficiency based on minimizing the dc current [23] and disturbing operating frequency [24] are presented. P&O methods have the advantages of simple structure, easy implementation, robustness to system parameters, and independent of real-time communication. However, such methods are troubled by the continuous oscillation and the tradeoff between the oscillation and convergence rate. Furthermore, the poor dynamic response of the output regulator also deteriorates the convergence rate of P&O method.

The output regulation of WPT system is usually realized by classical proportional–integral (PI) controller [17], [18], [19], [20], [25] or proportional–integral–differential (PID) controller [26]. Although the better control performance of PI/PID controller can be achieved by optimizing the gains, PI/ PID controller perform poorly in terms of the dynamic response due to their inherent linear characteristics, so that the system suffers from the unexpected power/voltage overshoot, oscillation and long setting time. With the variation of power/voltage command, load and coupling coefficient, the efficiency and stability of dynamic or static WPT system could be affected, thus further deteriorating the working conditions of batteries, motors, and other electrical loads. Aiming at that, a discrete sliding mode control scheme is proposed in [23] to achieve the fast output voltage regulation for S-S compensated WPT systems. The dynamic performance of output voltage regulation can be improved to a certain extent. A switching control strategy based on the switching behavior of primary converter is proposed in [27]. This method has the fast dynamic response and the strong robustness to external disturbance. Nonetheless, the modeling process is intricate, and the switching frequency is higher than the resonant frequency, which increases the system loss. Model predictive control (MPC) has been gradually considered for the application in WPT system due to its fast dynamic, simple parameter tuning and multiobjective optimization. This work in [28] proposes a continuous-control-set model predictive control (CCS-MPC) scheme to achieve the power flow regulation with fast dynamic response. However, it is not based on the dynamic model of WPT system, which exerts a negative impact on the dynamic response. In [29], a combination of finite-control-set model predictive control (FCS-MPC) and pulse density modulation is proposed, where the better dynamic response is realized by the rolling optimization of voltage output. In [30], a dynamic mathematical model-based FCS-MPC is proposed for achieving the fast voltage regulation. The fast response of output voltage regulator can be guaranteed. Nevertheless, it requires extra current sensors to sample the secondary coil current and the dc output current, thus increasing the system cost and complexity.

In this article, a novel control scheme based on FCS-MPC and P&O methods is proposed for the dynamic improvement and the efficiency optimization of WPT systems. First, for the dynamic improvement, a novel FCS-MPC with adaptive step-size and improved cost function is presented. The first-order extended state observer (ESO) is introduced to combine with FCS-MPC to avoid the use of extra current sensors. The proposed FCS-MPC has a reduced prediction horizon, which allows the low computational burden. A two-stage series prediction

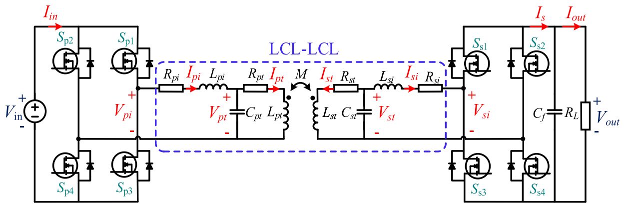

Fig. 1. Schematic diagram of the dual-side *LCL* compensated WPT system.

method is further proposed to reduce the computational burden of FCS-MPC method. Second, for the efficiency optimization, an adaptive P&O method is proposed to achieve MEET by minimizing the input dc current. The tracking process for the maximum efficiency point is divided into the tracking stage and oscillation stage, and an adaptive perturbation step-size is presented according to the state of tracking process to remove the tradeoff between the oscillation and convergence rate. Moreover, the cooperative control principle of the improved FCS-MPC and P&O methods is given to ensure the stable operation of the system. Finally, the effectiveness of the proposed scheme is verified on a 650-W WPT system platform.

II. MATHEMATICAL MODEL OF DUAL-SIDE *LCL* COMPENSATED WPT SYSTEM

The schematic diagram of the dual-side *LCL* compensated WPT system is shown in Fig. 1. V_{in} and I_{in} are the WPT system's dc input voltage and current. V_{out} and I_{out} are the WPT system's dc output voltage and current. L_{pt} and L_{st} are the self-inductances of primary and secondary coils. *M* denotes their mutual inductance and *k* denotes the coupling coefficient satisfying $k = M/\sqrt{L_{pt}L_{st}}$. L_{pi}, C_{pt}, L_{si}, and C_{st} are the dual-side compensation networks' components. R_{pi}, R_{si}, R_{pt}, and R_{st} are the equivalent parasitic resistances of L_{pi}, L_{si}, L_{pt}, and L_{st}. V_{pi} and V_{si} are the primary and secondary side converters' output voltages with the fixed frequency of f_s. The equivalent load resistance R_L is defined as the ratio of V_{out} to I_{out}. C_f denotes the filtering capacitor for system output.

A. Power Transfer Profile

Generally, f_s is set to the resonant frequency of compensation networks, and the corresponding angular frequency is expressed as

$$\begin{aligned}\omega = 2\pi f_s &= 1\Big/\sqrt{L_{pi}C_{pt}} = 1\Big/\sqrt{L_{pt}C_{pt}}\\ &= 1\Big/\sqrt{L_{si}C_{st}} = 1\Big/\sqrt{L_{st}C_{st}}.\end{aligned} \tag{1}$$

Due to the band-passing characteristic of compensation networks, fundamental harmonic approximation [5] is usually utilized to simplify the mathematical model. The fundamental components of V_{pi} and V_{si} can be described as

$$\dot{V}_{pi1} = \frac{2\sqrt{2}}{\pi}V_{in}\sin\left(\frac{\varphi_p}{2}\right)\angle 0,\ \dot{V}_{si1} = \frac{2\sqrt{2}}{\pi}V_{out}\sin\left(\frac{\varphi_s}{2}\right)\angle -\theta \tag{2}$$

where φ_p, φ_s and θ denote the phase shift angles of primary and secondary sides, which corresponds to three variables in the triple PSC. The corresponding switching signals and voltage waveforms are shown in Fig. 2. Primary and secondary converters' output currents and coil's currents are given by

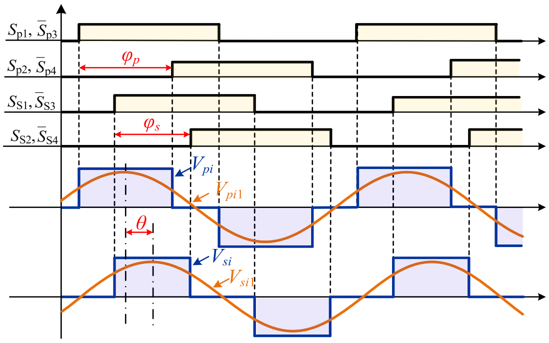

Fig. 2. Switching signals and voltage waveforms of the WPT system.

$$\begin{aligned}&\dot{I}_{pt} = \dot{V}_{pi1}/j\omega L_{pt}, \quad \dot{I}_{pi} = -M\dot{V}_{si1}/j\omega L_{pt}L_{st}\\ &\dot{I}_{st} = \dot{V}_{si1}/j\omega L_{st}, \quad \dot{I}_{si} = M\dot{V}_{pi1}/j\omega L_{pt}L_{st}.\end{aligned} \tag{3}$$

Ignoring the switching loss of inverters and the resistance loss of resonant networks, the active output power and reactive output power are given by

$$P_{out} = \mathrm{Re}\{\dot{V}_{si1}\dot{I}^*_{si}\} = \frac{8MV_{in}V_{out}}{\pi^2\omega L_{pt}L_{st}}\sin\left(\frac{\varphi_p}{2}\right)\sin\left(\frac{\varphi_s}{2}\right)\sin(\theta) \tag{4}$$

$$\begin{aligned}Q_{out} = \mathrm{Im}\{\dot{V}_{si1}\dot{I}^*_{si}\} = -j\frac{8MV_{in}V_{out}}{\pi^2\omega L_{pt}L_{st}}\sin\left(\frac{\varphi_p}{2}\right)\\ \sin\left(\frac{\varphi_s}{2}\right)\cos(\theta)\end{aligned} \tag{5}$$

where the outer phase shift angle θ is usually set to 90° for the zero reactive power and maximum efficiency transmission. Hence, the system output power is determined by the inner phase shift angles φ_p and φ_s, and there are countless combinations of φ_p and φ_s for the system power condition.

B. Dynamic Model for Voltage Control

For the CV output of dual-side *LCL* compensated WPT system using an active rectifier, a simple dynamic model of output voltage is established and expressed via

$$C_f\frac{dV_{out}}{dt} = I_s - I_{out}. \tag{6}$$

Through averaging (6), the dynamic voltage model can be transformed into [30]

$$\frac{dV_{out}}{dt} = \frac{2\sqrt{1-\cos(\varphi_s)}}{C_f\pi}I_{siRMS} - \frac{1}{C_f}I_{out} \tag{7}$$

where I_{siRMS} is the root-mean-square (rms) value of I_{si}. Discretizing (7) using forward Euler method yields

$$V_{out}(k+1) = \frac{T_p}{C_f}\left[\frac{2I_{siRMS}(k)}{\pi}\sqrt{1-\cos(\varphi_s(k))} - I_{out}(k)\right]$$

$$+ V_{out}(k) \tag{8}$$

where k denotes the controlling instant and T_p denotes the voltage control period. It can be seen from (8) that the regulation of system voltage output can be realized by controlling the inner phase shift angle φ_s.

C. Efficiency Analysis

To track the maximum energy efficiency for WPT system, the power losses and system efficiency of WPT system should be analyzed. The power losses of WPT system mainly composed of the resistance loss of resonant networks, and the conducting and switching losses of inverter and active rectifier [31], [32]. Then, the efficiency of WPT system can be described as

$$\eta = \frac{P_{out}}{P_{in}} \approx \frac{P_{out}}{P_{out} + P_{res} + P_{inv} + P_{rec}} \tag{9}$$

where P_{in} is the system input power, P_{res} is the resistance loss of resonant networks, P_{inv} is the inverter loss, and P_{rec} is the rectifier loss. The resistance loss of resonant networks can be calculated by

$$P_{res} = I_{pi}^2 R_{pi} + I_{si}^2 R_{si} + I_{pt}^2 R_{pt} + I_{st}^2 R_{st}. \tag{10}$$

In reported MEET schemes in [18], [19], and [20], the converter losses of WPT system are ignored and only the resistance loss of resonant networks is considered. In these methods, assuming that $P_{inv} = P_{rec} = 0$ and $\theta = 90°$ yields

$$\begin{aligned}\eta &\approx \tfrac{P_{out}}{P_{out}+P_{res}}\\ &= \tfrac{\omega L_{st} L_{pt} V_{pi1} V_{si1}}{M\left[V_{pi1}^2 (R_{si}+L_{st}^2 R_{pt})+V_{si1}^2\left(R_{pi}+L_{pt}^2 R_{st}\right)\right]+\omega L_{st} L_{pt} V_{pi1} V_{si1}}.\end{aligned} \tag{11}$$

Defining G as the ratio of V_{si1} to V_{pi1}. By solving $d\eta/dG = 0$, the optimal G for MEET can be derived as

$$G_{opt} = \sqrt{(R_{si} + L_{st}^2 R_{pt}) \big/ (R_{pi} + L_{pt}^2 R_{st})}. \tag{12}$$

By substituting (2) into (12), the optimal relationship between φ_p and φ_s can be obtained as

$$\varphi_p = 2 \arcsin \left[\frac{V_{out}}{V_{in}} \sqrt{\frac{R_{si} + L_{st}^2 R_{pt}}{R_{pi} + L_{pt}^2 R_{st}}} \cdot \sin\left(\frac{\varphi_s}{2}\right) \right]. \tag{13}$$

However, the maximum efficiency point is tracked according to (13) by minimizing the resistance loss of resonant networks, where the dual-side converter losses are ignored. Moreover, this method also depends on system parameters. The ignored converter losses and mismatched parameters may cause the calculation results to deviate from the actual value.

On the other hand, the power losses of dual-side converters mainly contain the conducting and switching losses, which can be expressed as

$$\begin{cases} P_{inv} = P_{inv\_con} + P_{inv\_\mathrm{sw}} \\ P_{rec} = P_{rec\_con} + P_{rec\_\mathrm{sw}} \end{cases} \tag{14}$$

where P_{inv_con} and P_{rec_con} denote the conducting losses of inverter and active rectifier, and P_{inv_sw} and P_{rec_sw} denote the switching losses of inverter and active rectifier, which can be calculated by

$$\begin{cases} P_{inv\_con} = 2I_{pi}^2 R_{DS} + 2\sqrt{2} V_f I_{pi} \left[1 - \sin(\varphi_p/2)\right] / \pi \\ P_{rec\_con} = 2I_{si}^2 R_{DS} + 2\sqrt{2} V_f I_{si} \left[1 - \sin(\varphi_s/2)\right] / \pi \\ P_{inv\_\mathrm{sw}} = 2\sqrt{2} V_{in} I_{pi} f_s \cos\left(\frac{\varphi_p}{2}\right) \left(\frac{E_{sw\_\mathrm{on}} + E_{sw\_\mathrm{off}}}{V_R I_R} + \frac{Q_{RR}}{I_{RD}}\right) \\ P_{rec\_\mathrm{sw}} = 2\sqrt{2} V_{out} I_{si} f_s \cos\left(\frac{\varphi_s}{2}\right) \left(\frac{E_{sw\_\mathrm{on}} + E_{sw\_\mathrm{off}}}{V_R I_R} + \frac{Q_{RR}}{I_{RD}}\right) \end{cases} \tag{15}$$

where R_{DS} denotes the equivalent ON-state resistance, V_f denotes the threshold voltage, E_{sw_on} and E_{sw_off} denote the turn ON and turn OFF losses of MOSFET, V_R and I_R denote the drain-source voltage and current of MOSFET, and Q_{RR} and I_{RD} denote the reverse recovery charge and the reference current of the diode. Obviously, the system efficiency can be calculated by combining (9), (10), (14), and (15), but it is difficult to obtain the relationship between phase shift angles to track the maximum efficiency point, because of such complex nonlinear efficiency equation about phase shift angles.

III. IMPROVED FCS-MPC SCHEME FOR DYNAMIC IMPROVEMENT

MPC has been widely applied in fields of power converters and drivers because of its fast dynamic, simple parameter tuning and multiobjective optimization [33], which is also gradually considered for the application of WPT systems. In this section, a novel FCS-MPC is proposed for the dynamic improvement of output voltage regulator, and its performance merits are listed as follows.

1) Fast dynamics: The operating mechanism of FCS-MPC, and the proposed adaptive step-size and cost function allow the faster regulation for the output voltage of WPT system.
2) Current sensorless control: A first-order ESO is introduced in dynamic voltage model to estimate the uncertain output current, so that the extra current sensors used in reported methods in [30] can be avoided.
3) Low computation burden: The rolling calculations of the proposed FCS-MPC are few in one control period, and the proposed two-stage series prediction can further alleviate the computation burden.

The operation mechanisms and details of the proposed FCS-MPC are described as the following content.

A. Current Sensorless Model With ESO for FCS-MPC

To compensate one-sample time delay in digital control, the typical two-step prediction scheme presented in [34] is adopted. Based on the one-step prediction of (8), the second step prediction of system output voltage can be expressed as

$$\begin{aligned} &V_{out}(k+2)\\ &= \frac{T_p}{C_f}\left[\frac{2\sqrt{1-\cos(\varphi_s(k+1))}}{\pi} I_{siRMS}(k+1) - I_{out}(k+1)\right]\\ &\quad + V_{out}(k+1). \end{aligned} \tag{16}$$

The dc output current and the rms value of I_{si} can be considered as constant in one control period and yields

$$I_{siRMS}(k+1) = I_{siRMS}(k), \quad I_{out}(k+1) = I_{out}(k). \tag{17}$$

Substituting (8) and (17) into (16) yields

$$\begin{aligned} &V_{out}(k+2) \\ &= \frac{2T_p\left(\sqrt{1-\cos(\varphi_s(k))}+\sqrt{1-\cos(\varphi_s(k+1))}\right)}{C_f\pi} \\ &\quad \times I_{siRMS}(k) - 2T_p\frac{I_{out}(k)}{C_f} + V_{out}(k). \end{aligned} \tag{18}$$

It is obvious that the discrete dynamic model (18) requires not only the output voltage sampling but also extra current sensors for the rms value of I_{si} and the output current I_{out}. The utilization of current sensors undoubtedly increases the system cost and size. Aiming at that, a first-order linear ESO is introduced to avoid the utilization of current sensors.

First, the dynamic voltage model (7) is a first-order single-input single-output system, and its state-space model is given by

$$\frac{d}{dt}\begin{bmatrix} x_1 \\ f \end{bmatrix} = \begin{bmatrix} 0 & 1 \\ 0 & 0 \end{bmatrix}\begin{bmatrix} x_1 \\ f \end{bmatrix} + \begin{bmatrix} b_0 \\ 0 \end{bmatrix}u + \begin{bmatrix} 0 \\ 1 \end{bmatrix}h \tag{19}$$

where x_1 denotes the state variable, u denotes the system input, b_0 denotes the system input gain, and f denotes the total disturbance satisfying $df/dt = h$. According to (7), the above parameters can be expressed as

$$\begin{cases} x_1 = V_{out} \\ b_0 = 2I_{siRMS}/(\pi C_f) \\ u = \sqrt{1-\cos(\varphi_s)} \\ f = -I_{out}/C_f. \end{cases} \tag{20}$$

The linear ESO can be represented as

$$\frac{d}{dt}\begin{bmatrix} z_1 \\ z_2 \end{bmatrix} = \begin{bmatrix} 0 & 1 \\ 0 & 0 \end{bmatrix}\begin{bmatrix} z_1 \\ z_2 \end{bmatrix} + \begin{bmatrix} b_0 \\ 0 \end{bmatrix}u + \begin{bmatrix} \beta_1 \\ \beta_2 \end{bmatrix}[x_1 - z_1] \tag{21}$$

where z_1 is the estimation of the state variable, z_2 is the estimation of the total disturbance, and β_1 and β_2 are adjustable gains of linear ESO.

Defining the estimation errors as $\varepsilon_1 = x_1 - z_1$ and $\varepsilon_2 = f - z_2$, the state-space model of estimation errors is expressed via

$$\begin{bmatrix} p\varepsilon_1 \\ p\varepsilon_2 \end{bmatrix} = \begin{bmatrix} -\beta_1 & 1 \\ -\beta_2 & 0 \end{bmatrix}\begin{bmatrix} \varepsilon_1 \\ \varepsilon_2 \end{bmatrix} + \begin{bmatrix} 0 \\ h \end{bmatrix}. \tag{22}$$

If the adjustable gains satisfy that $\beta_1 > 0$ and $\beta_2 > 0$, the Hurwitz stability criterion is satisfied and the estimation errors can converge exponentially to zero. Defining the coefficient ω_n as the observer bandwidth, the adjustable gains of linear ESO can be obtained as

$$\beta_1 = 2\omega_n, \quad \beta_2 = \omega_n^2. \tag{23}$$

The transfer function between estimated total disturbance and actual total disturbance can be described as

$$H(s) = \frac{z_2(s)}{f(s)} = \frac{\omega_n^2}{s^2 + 2\omega_n s + \omega_n^2}. \tag{24}$$

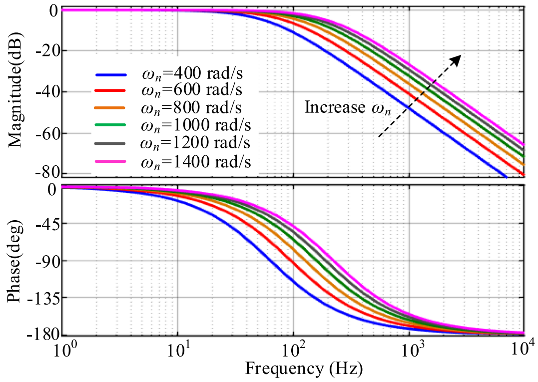

Fig. 3. Bode diagram of transfer function $H(s)$ between estimated and actual total disturbances with different ω_n.

As seen from (24), the linear ESO for estimating the total disturbance has the low-pass filtering characteristics. The Bode diagram of transfer function $H(s)$ between estimated and actual total disturbances with different ω_n is shown in Fig. 3. It can be seen that the larger the observer bandwidth ω_n, the faster the convergence rate. However, a large observer bandwidth ω_n will make the observer sensitive to noise. This means for the selection of ω_n, a tradeoff between the convergence rate and antinoise ability should be considered. In this article, ω_n is set to 1000 rad/s by extensive simulations and experimental results.

By substituting (20) into (21) and discretizing, the discrete linear ESO for estimating the uncertain output current can be obtained as

$$\begin{cases} z_1(k+1) = z_1(k) + T_P z_2(k) + T_P\beta_1\left[V_{out}(k) - z_1(k)\right] \\ + \frac{2T_P}{C_f\pi}I_{siRMS}(k)\cdot\sqrt{1-\cos(\varphi_s(k))} \\ z_2(k+1) = z_2(k) + T_P\beta_2\left[V_{out}(k) - z_1(k)\right] \end{cases} \tag{25}$$

where for achieving the current sensorless control, $I_{siRMS}(k)$ can be calculated by

$$I_{siRMS}(k) = \frac{2\sqrt{2}MV_{in}}{\pi\omega L_{pt}L_{st}}\sin\left(\frac{\varphi_p(k)}{2}\right). \tag{26}$$

Although the acquisition of $I_{siRMS}(k)$ requires the system parameters, the model errors caused by mismatched parameters can be included to the estimated total disturbance $z_2(k+1)$ and compensated.

Combining (18) and (25), the current sensorless model with ESO for FCS-MPC can be described as

$$\begin{aligned} &V_{out}(k+2) = \\ &\frac{4\sqrt{2}T_pMV_{in}\left(\sqrt{1-\cos(\varphi_s(k))}+\sqrt{1-\cos(\varphi_s(k+1))}\right)}{\pi^2\omega L_{pt}L_{st}C_f} \\ &\times\sin\left(\frac{\varphi_p(k)}{2}\right) + 2T_pz_2(k+1) + V_{out}(k). \end{aligned} \tag{27}$$

B. Operating Principle of FCS-MPC

According to (27), $V_{out}(k+2)$ could be predicted by using the dynamic voltage model about $V_{out}(k)$, $\varphi_s(k)$, $\varphi_s(k+1)$, $\varphi_p(k)$,

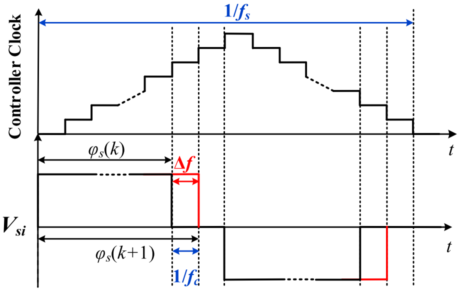

Fig. 4. Demonstration of the finest phase shift value Δf for the digital controller.

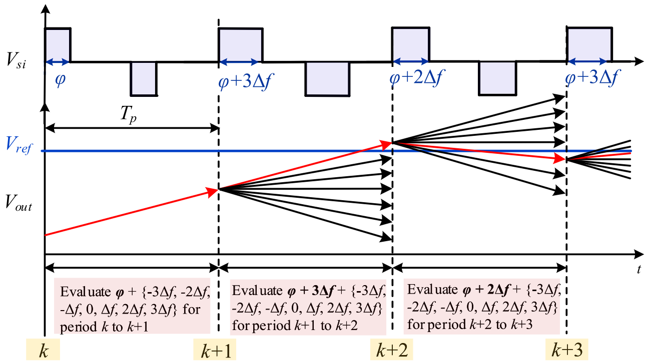

Fig. 5. Operation mechanism of the proposed FCS-MPC, where n is set to 7.

and $z_2(k+1)$ as

$$V_{out}(k+2) = f\left\{V_{out}(k), \varphi_s(k), \varphi_s(k+1), \varphi_p(k), z_2(k+1)\right\} \tag{28}$$

where $\varphi_s(k+1) = \varphi_s(k) + \Delta\varphi(k)$. $V_{out}(k+2)$ can be regulated to the reference value by selecting the optimal value of $\Delta\varphi(k)$. The optimal $\Delta\varphi(k)$ is obtained by the predicted behaviors and the rolling calculation, and the cost function to calculate the fitness value is expressed as (29). Note that (29) is not the final cost function, but a simple one to make the operation mechanism of FCS-MPC easy to understand

$$J = \left(V_{out}(k+2) - V_{ref}\right)^2. \tag{29}$$

The phase shift angle φ_s varies continuously between 0 and π rad, which does not possess discrete states of power converters. The phase shift angle φ_s should be discretized for the digital implementation. The Δf is defined as the finest phase shift value that can be achieved in a digital controller, as elaborated in Fig. 4. The discretization precision should be decided by the clock frequency of digital controller, following that

$$\Delta f = \frac{f_s}{f_c} \times 2\pi \tag{30}$$

where f_c is the clock frequency of digital controller. Then, the selection range of φ_s can be divided into $n_{\max} = (\pi/\Delta f + 1)$ segments and expressed as

$$\varphi_s \in \left\{0, \Delta f, 2\Delta f, 3\Delta f, \ldots, \pi\right\}. \tag{31}$$

To realize the rolling calculation, the FCS of $\Delta\varphi$ is defined as

$$\Delta\varphi \in \left\{-\frac{(n-1)\Delta f}{2}, \ldots, -\Delta f, 0, \Delta f, \ldots, \frac{(n-1)\Delta f}{2}\right\} \tag{32}$$

where n (n is odd and $n \geq 3$) denotes the number of elements of FCS. It is obvious that 0 is the center of FCS and the difference between each adjacent element is Δf.

The operation mechanism of FCS-MPC is elaborated in Fig. 5, where n is set as 7. At the control instant k, the initial value of φ_s is defined as φ. In the control interval k to $k+1$, the FCS of $\varphi_s(k+1)$ is calculated by $\varphi_s(k+1) = \varphi_s(k) + \Delta\varphi = \varphi + \{-3\Delta f, -2\Delta f, -\Delta f, 0, \Delta f, 2\Delta f, 3\Delta f\}$, and utilized for the rolling calculations by dynamic voltage model (27) and minimizing the cost function (29) to find the optimal phase shift angle $\varphi_s(k+1) = \varphi + 3\Delta f$. Hence, the value of $\varphi + 3\Delta f$ is applied at the time instant $k+1$ for φ_s. Similarly, in the control interval $k+1$ to $k+2$, the FCS of $\varphi_s(k+2)$ is calculated by $\varphi_s(k+2) = \varphi_s(k+1) + \Delta\varphi = \varphi + 3\Delta f + \{-3\Delta f, -2\Delta f, -\Delta f, 0, \Delta f, 2\Delta f, 3\Delta f\}$. The same process for the optimal phase shift angle is repeated, and the value of $\varphi + 2\Delta f$ is obtained and applied at time instant $k+2$ for φ_s. In the control interval $k+2$ to $k+3$, $\varphi_s(k+2) = \varphi + 3\Delta f$ takes the smallest fitness, which is applied at the time instant $k+3$. Such a process is carried out in each control period.

C. Two-Stage Series Prediction for Low Computational Burden

The execution time of the algorithm is crucial for the digital implementation. In the FCS-MPC, the element number n of FCS corresponds to the number of rolling calculations. Increasing n leads to the greater control performance and the higher computational burden. This means there is a tradeoff between control performance and computational burden. To relieve the computational burden, a two-stage series prediction method is proposed for FCS-MPC and it has a two-stage prediction process. Two FCSs for different prediction processes are given by

$$\Delta\varphi_1 \in \left\{-\frac{(n-3)\Delta f}{2}, \ldots, -2\Delta f, 0, 2\Delta f, \ldots, \frac{(n-3)\Delta f}{2}\right\} \tag{33}$$

$$\Delta\varphi_2 \in \left\{-\Delta f, \Delta f\right\} \tag{34}$$

where (33) and (34) denote the FCSs for the first prediction and the second prediction. The cost functions of the first and second predictions are the same.

For ease of understanding, the case of the period k to $k+1$ in Fig. 5 is taken as an example to illustrate the operation mechanism of two-stage series prediction method, as depicted in Fig. 6. At the control instant k, the initial value of φ_s is defined as φ for the first prediction. In the first stage prediction process, the FCS of $\varphi_s(k+1)$ is calculated by $\varphi_s(k+1) = \varphi_s(k) + \Delta\varphi_1 = \varphi + \{-2\Delta f, 0, 2\Delta f\}$, which is utilized for the rolling calculations to find the optimal phase shift angle. $\varphi + 2\Delta f$ takes the smallest fitness of J_1, so it is set as the initial value of the second prediction. In the second stage prediction process, the

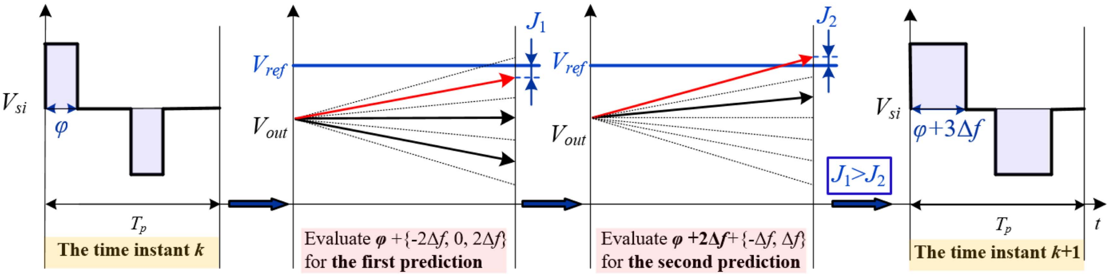

Fig. 6. Operation mechanism of the proposed two-stage series prediction method.

TABLE I
ROLLING CALCULATION NUMBER OF SINGLE-STEP SCHEME AND TWO-STAGE SERIES SCHEME FOR SAME PERFORMANCE

Method	Rolling calculation number for same performance					
Single-step method	3	7	11	15	…	n
Two-stage series method	3	5	7	9	…	$(n+3)/2$

FCS of $\varphi_s(k+1)$ is recalculated by $\varphi_s(k+1) = \varphi + 2\Delta f + \Delta\varphi_2 = \varphi + 2\Delta f + \{-\Delta f, \Delta f\}$. The same calculation process is repeated, and $\varphi + 3\Delta f$ takes the smallest fitness of J_2 and is taken as the optimal phase shift angle. By comparing J_1 and J_2, $\varphi + 3\Delta f$ is applied at the time instant $k + 1$.

Obviously, the two-stage series FCS-MPC only requires five rolling calculations to achieve the control performance of seven rolling calculations of single-step scheme. The rolling calculation number of single-step scheme and two-stage series scheme for the same performance is shown in Table I. It can be seen that the proposed two-stage series scheme only takes $(n + 3)/2$ number of rolling calculations to realize the same as the performance of single-step scheme with n number of rolling calculations. Compared with the single-step method, it is able to reduce $(n - 3)/2$ number of rolling calculations.

Especially for the case where the multistep rolling computations is required, the two-stage series scheme can markedly reduce the computational burden. In this article, n is selected as 11, which indicates only seven rolling calculations are required for the proposed FCS-MPC method.

D. *Adaptive Step-Size and Improved Cost Function*

According to the above operating principle of FCS-MPC, the step-size Δf is related to the dynamic response and steady accuracy of the WPT system. Because Δf is the finest phase shift value for the digital controller, the dynamic response can be ensured only by increasing n, i.e., the number of rolling calculations. However, this could undoubtedly increase the computational burden of the digital controller. To solve this problem, an adaptive step-size Δ_{adp} is proposed and expressed as

$$V_{err} = \begin{cases} V_m, & V_m \le |V_{ref} - V_{out}(k)| \\ |V_{ref} - V_{out}(k)|, & |V_{ref} - V_{out}(k)| < V_m \end{cases} \tag{35}$$

$$\Delta_{adp} = (1 + \lambda V_{err}) \cdot \Delta f \tag{36}$$

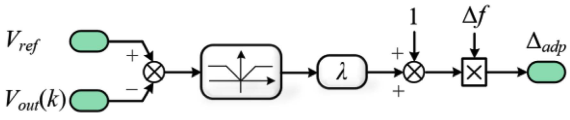

Fig. 7. Diagram of the adaptive step-size.

where V_m denotes the saturation voltage error, and λ denotes the gain of voltage error, which is proportional to the adaptive step-size. From (35) and (36), Δ_{adp} varies with the difference between the actual and reference voltages. Δ_{adp} increases as that the actual voltage deviates from reference value. When the output voltage converges to the reference value, Δ_{adp} is equal to Δf. The large values of λ and V_m can enhance the tracking speed for the voltage reference, but their too large values may lead to steady-state chattering while the system suffers from the external disturbance. In this article, λ and V_m are set as 1 and 40 V, respectively. The diagram of adaptive step-size is shown in Fig. 7.

To further accelerate the convergence rate, an improved cost function is proposed and described as

$$J = (V_{out}(k+2) - V_{ref})^2 + \alpha(V_{out}(k+2) - V_{out}(k))^2 \tag{37}$$

where it is obvious that the improved cost function contains two terms and α ($\alpha > 0$) is the weighting factor of the second term. The first term is relevant to the difference between the predicted and reference voltages, which plays a central role when the actual voltage is far away from the reference value. The second part reflects the difference between the predicted and actual voltages. It gradually takes effect as the actual voltage approaches the reference voltage, which is responsible for reducing the voltage deviation. The addition of the second term is conducive to accelerate the convergence rate. The tuning of weighting factor α is crucial to the control performance of the proposed FCS-MPC, and the artificial neural network method [35] is a great method to tune the weighting factor.

E. *Flowchart of the Proposed FCS-MPC*

According to the above-mentioned analysis, the flowchart of the proposed FCS-MPC is concluded in Fig. 8, and its detailed implementation steps are described as follows.

Step 1: First, measure the dc output voltage $V_{out}(k)$ and initialize $J_1 = J_2 = \infty$. Calculate the total disturbance $z_2(k + 1)$ by (25) and the adaptive step-size Δ_{adq} by (35) and (36).

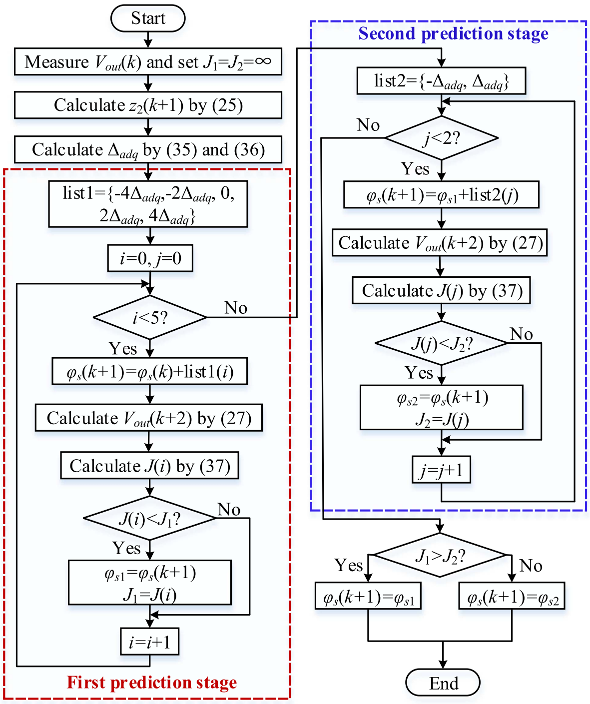

Fig. 8. Flowchart of the proposed FCS-MPC.

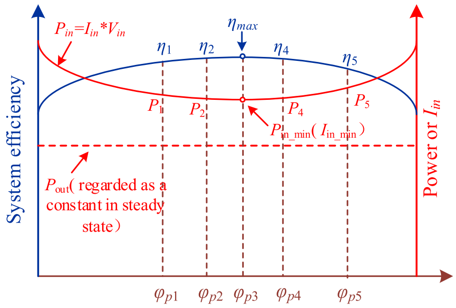

Fig. 9. Relationship between efficiency, power/current, and φ_p.

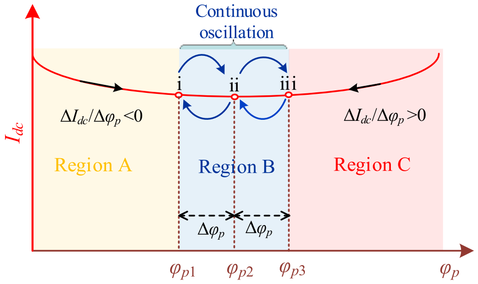

Fig. 10. Operation mechanism of the P&O method for WPT systems.

Step 2: Initialize *i* and *j* for the rolling calculations of two-stage predictions. Arrange the FCS $\{-4\Delta_{adq}, -2\Delta_{adq}, 0, 2\Delta_{adq}, 4\Delta_{adq}\}$ for the first stage prediction and enter the first stage prediction process. Calculate the predicted voltage V_{out} $(k+2)$ by (27) and cost function *J*(*i*) by (37). Judge whether *i* is less than 5. If so, $i = i + 1$ and repeat the rolling calculation. If not, find the optimal phase angle φ_{s1} with the smallest fitness of J_1.

Step 3: After *Step* 2, enter the second stage prediction process. Arrange the FCS $\{-\Delta_{adq}, \Delta_{adq}\}$ for the second stage prediction. Calculate the predicted voltage $V_{out}(k+2)$ by (27) and cost function *J*(*j*) by (37). Judge whether *j* is less than 2. If so, *j* $= j + 1$ and repeat the rolling calculation. If not, find the optimal phase angle φ_{s2} with the smallest fitness of J_2.

Step 4: Finally, judge whether J_1 is greater than J_2. If so, φ_{s1} is applied in the next period. If not, φ_{s2} is applied in the next period. This means the phase shift angle φ_s for the next period has been determined.

IV. ADAPTIVE P&O METHOD FOR EFFICIENCY OPTIMIZATION

In Section III, the proposed FCS-MPC is adopted to dynamically adjust the inner phase shift angle φ_s of active rectifier for the CV output. The variation of φ_s will lead to the deviation of maximum efficiency point. Hence, on the premise of ensuring the stability of output voltage, an effective control scheme is crucial to adjust the inner phase shift angle φ_p of the primary inverter for MEET.

A. Conventional P&O Method for MEET

According to analysis in Section III-C, it is difficult to solve the phase shift angle φ_p to track the maximum efficiency point with such a complex nonlinear trigonometric function about phase shift angles. Fortunately, the system output power can be regarded as constant in the steady state, and the input dc current I_{in} can be regulated by adjusting the phase shift angle φ_p. Moreover, because the input voltage is constant, the minimum system input power P_{in} can be achieved by minimizing the input dc current I_{in}. Hence, the P&O method-based PSC can be adopted to minimize the system input current I_{in} by perturbing the phase shift angle φ_p [23], [30]. The relationship between efficiency, power/current, and φ_p is depicted in Fig. 9.

The operation mechanism of the P&O method for WPT systems is elaborated in Fig. 10. When the system is in regions A and C, I_{in} can be continuously reduced by increasing or decreasing φ_p by the perturbation step-size $\Delta\varphi_p$. When the system enters region B, the state of φ_p becomes a three-point oscillation stage between points i, ii, and iii, which means the optimal φ_p for the MEET is found. Note that the stability of output voltage has the highest priority. If V_{out} is lower than the reference value, φ_p should be increased immediately.

The flowchart of the conventional P&O method is shown in Fig. 11. Obviously, the conventional P&O method for MEET of WPT systems is simple, effective, and independent of system parameters. However, the continuous injection of perturbation leads to the inevitable oscillation, which may increase the power loss and reduce the system stability. Moreover, there is a tradeoff about the selection of the perturbation step-size $\Delta\varphi_p$ between the oscillation and convergence rate.

B. Adaptive P&O Method for MEET

To conquer the contradiction between the dynamic and steady-state performance of conventional P&O method, an adaptive P&O method is proposed in this section.

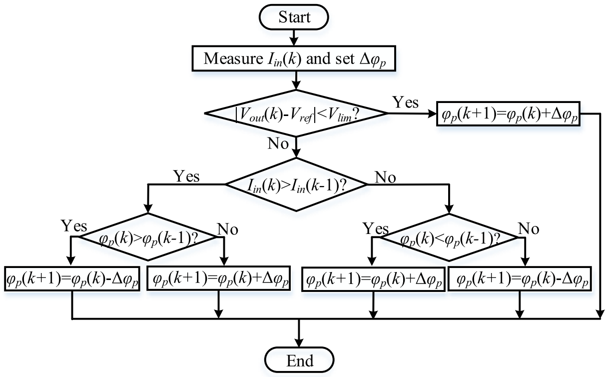

Fig. 11. Flowchart of the conventional P&O method.

TABLE II
DETERMINATION OF THE N VALUES

$\Delta I_{in}(k)$	$\Delta\varphi_p(k)$	$N(k)$
>0	>0	−1
>0	<0	+1
<0	>0	+1
<0	<0	−1

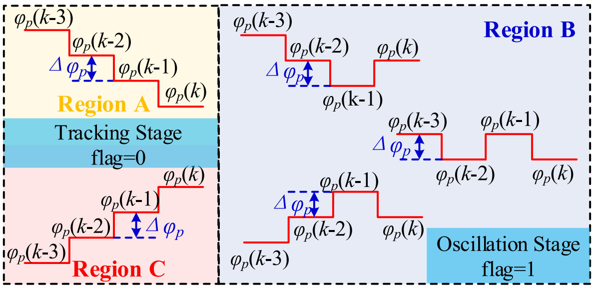

Fig. 12. Trend of φ_p in t ($t = 3$) number of consecutive periods.

1) Determination of Tracking Stage: In this method, the tracking process for maximum efficiency point is divided into the tracking stage (flag = 0) and the oscillation stage (flag = 1) by introducing the variable N to record the direction of disturbance. The value of N is decided by the signs of input current variation $\Delta I_{in}(k) = I_{in}(k) - I_{in}(k-1)$ and angle variation $\Delta\varphi_p(k) = \varphi_p(k) - \varphi_p(k-1)$, as shown in Table II. The system state can be obtained by detecting the sum of N in t number of consecutive periods, which can be described as

$$\text{sum} = \left|\sum_{i=0}^{t-1} N(k-i)\right| \begin{cases} = t, & \text{oscillation stage} \\ < t, & \text{tracking stage} \end{cases} \tag{38}$$

where t is an integer not less than 3.

To elaborate the determination of system state intuitively, the trend of the phase shift value φ_p in t number of consecutive control periods is shown in Fig. 12, where t is set as 3 for easy understanding. In the tracking stage (region A or region B), three consecutive N are either positive or negative. Hence, the absolute value of the sum of all three N is 3. After reaching the maximum efficiency point, the oscillation starts. The operating point will move two times in one direction and move one time in the opposite direction, so that the absolute value of the sum of all three N is always less than 3. So, the oscillation stage can be detected.

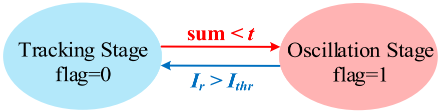

Fig. 13. State switching conditions for adaptive P&O method.

2) Adaptive Perturbation Step-Size: When the system enters region A or region C, the tracking process is in the tracking stage, where the maximum efficiency point has not been found. The perturbation step-size should be large to ensure the fast convergence to the maximum efficiency point. However, when the system enters region B, which means the maximum efficiency point has been found. The tracking stage is in the oscillation stage, where a small perturbation step-size should be set to reduce the power loss and ensure the system stability.

Hence, an adaptive perturbation step-size is proposed according to different system stages. In the tracking stage, a large perturbation size Δ_{const} is selected to ensure the fast convergence to the oscillation stage. When the system enters the oscillation stage, the large perturbation size Δ_{const} is continuously decreased by Δ_{step} in each control period until it reaches a small value of $\Delta_{\min}$. The small perturbation size $\Delta_{\min}$ is maintained until a considerable load variation occurs in response to the deviation of maximum efficiency point caused by a small or slow load variation or external disturbance. Moreover, because the sampling error or external disturbance may cause the system jump from the oscillation stage with the step-size $\Delta_{\min}$ to the tracking stage with the step-size Δ_{const} unexpectedly, $N(k)$ is set as 0 when the perturbation size is equal to $\Delta_{\min}$ so that the system state can be locked in the oscillation stage with the step-size $\Delta_{\min}$. Although the oscillation still exists in the adaptive P&O method, $\Delta_{\min}$ is so small that the oscillation can be ignored.

3) State Switching Conditions for Adaptive P&O Method: The design of the system state switching conditions is vital for the adaptive P&O method. The switching condition from the tracking stage to the oscillation stage that the value of sum is reduced from 3 to less than 3 can be easily obtained. When a considerable load variation or external disturbance occurs, the oscillation stage should be switched to the tracking stage for reaching the maximum efficiency working point within the shortest time possible. The change rate of input current I_{in} is introduced to judge whether a considerable system load change or external disturbance occurs, which is defined as

$$I_r = |\Delta I_{in}(k)/I_{inrated}| \tag{39}$$

where $I_{in\ \text{rated}}$ is the rated dc input current value. If $I_r \geq I_{thr}$, this means that the maximum efficiency point has shifted significantly, and the perturbation step-size should be switched to Δ_{const}. To sum up, the state switching conditions for the adaptive P&O method are depicted in Fig. 13.

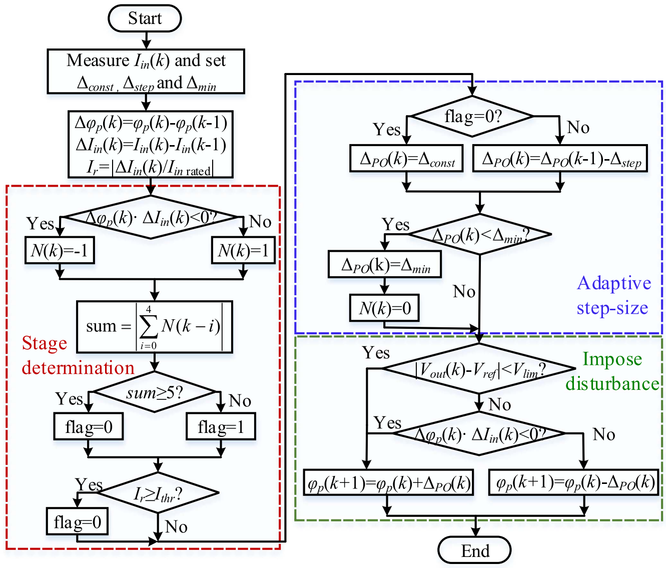

Fig. 14. Flowchart of the adaptive P&O method.

4) Flowchart of Adaptive P&O Method: The flowchart of the conventional P&O method is shown in Fig. 14, where t is set as 5, and its detailed implementation steps are described as follows.

Step 1: First, measure the dc input current I_{in} (k) and initialize parameters $\Delta_{const,}$ Δ_{step} and $\Delta_{\min}$ of the adaptive step-size. Calculate the variations $\Delta\varphi_p(k)$ and $\Delta I_{in}(k)$, and the change rate I_r.

Step 2: Enter the stage determination process. Determine the value of $N(k)$ according to Table I and calculate sum according to (38). Judge whether sum is less than t and I_r is less than $I_{in\ \mathrm{rated}}$. If so, flag $= 1$, which corresponds to the oscillation stage. If not, flag $= 0$, which corresponds to the tracking stage.

Step 3: Set the adaptive step-size according to the value of flag. If flag $= 1$, $\Delta_{PO}(k)$ is assigned as a large value of Δ_{const}. If flag $= 0$, $\Delta_{PO}(k)$ is obtained by subtracting Δ_{step} from $\Delta_{PO}(k{-}1)$. Judge whether $\Delta_{PO}(k)$ is less than $\Delta_{\min}$. If so, $\Delta_{PO}(k)$ is assigned as $\Delta_{\min}$ and $N(k) = 0$.

Step 4: Finally, enter the disturbance imposing process. The stable output voltage should be first ensured. Hence, while $|V_{out}(k) - V_{ref}| > V_{lim}$, $\varphi_p(k + 1)$ should be increased by $\Delta_{PO}(k)$ to provide the required output power. In other cases, judging whether the product of $\Delta I_{in}(k)$ and $\Delta\varphi_p(k)$ is less than 0. If so, $\varphi_p(k + 1) = \varphi_p(k) + \Delta_{PO}(k)$. If not, $\varphi_p(k + 1) = \varphi_p(k) - \Delta_{PO}(k)$.

C. Cooperative Control Principle of FCS-MPC and Adaptive P&O

The time delay caused by sampling circuit, communication device, and digital calculation may cause the problems of system instability or performance degradation in many power electronic systems, especially for systems where two or more digital controllers are required. Moreover, since the system output power is jointly determined by phase shift angles φ_p and φ_s, the simultaneous adjustment of φ_p and φ_s may result in the system instability or power oscillation. Hence, considering the above factors, the simultaneous adjustment of φ_p and φ_s should be avoided. Furthermore, the fast adjustment of the phase shift angle φ_s is responsible for the fast response of output regulation, so the proposed FCS-MPC has the highest priority with the control period T_p for the dynamic improvement of system output. Then, based on the dynamic improvement of the output voltage provided by FCS-MPC, the phase shift angle φ_p is relatively slowly adjusted with the control period T_r ($T_r << T_p$) to achieve the dynamic MEET robust to system parameters by the adaptive P&O method. The block diagram of the joint control strategy using improved FCS-MPC and P&O methods for WPT systems is shown in Fig. 15.

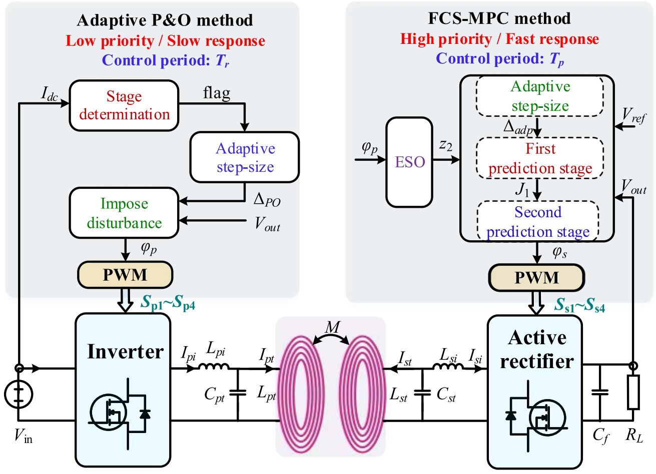

Fig. 15. Block diagram of the proposed control scheme for WPT system.

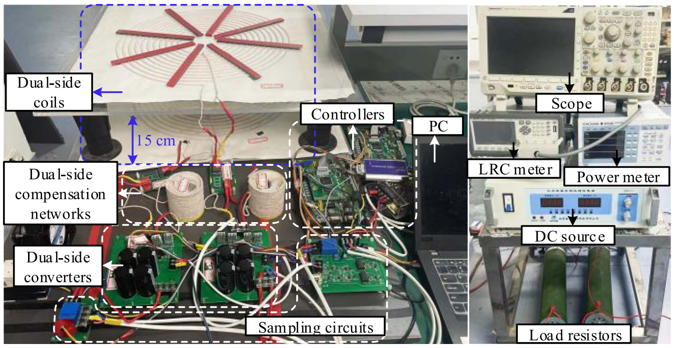

Fig. 16. Experiment platform of the WPT system.

V. EXPERIMENTAL RESULTS

A. Experimental Setup

The experimental platform of the dual-side *LCL* compensated WPT system is built to verify the capability of the proposed control scheme, as depicted in Fig. 16. The prototype includes a dc source, an *LCL–LCL* resonant network, dual-side converters, controllers, sampling circuits and load resistances. The coupled coils are made by the Litz wire composed of 300 varnished wires

TABLE III
CIRCUIT PARAMETERS OF THE WPT SYSTEM

Parameter	Value	Parameter	Value	Parameter	Value
V_{in}	300 V	V_{out}	300 V	C_{pt}	71.7 nF
L_{pt}	48.2 μH	R_{pt}	91.5 mΩ	C_{st}	71.8 nF
L_{st}	49.4 μH	R_{st}	87.9 mΩ	M	12.0 μH
L_{pi}	49.4 μH	R_{pi}	66.6 mΩ	f_s	85 kHz
L_{si}	49.0 μH	R_{si}	64.6 mΩ	C_f	470 μF

TABLE IV
CONTROL PARAMETERS OF THE PROPOSED FCS-MPC AND ADAPTIVE P&O

	Parameter	Value	Parameter	Value
Parameters of FCS-MPC	T_p	50 μs	V_m	40 V
	f_s	20 kHz	n	11
	Δf	0.204°	λ	1
	ω_n	1000 rad/s	α	4
Parameters of adaptive P&O method	T_r	100 ms	Δ_{const}	15°
	V_{lim}	2 V	Δ_{step}	1.5°
	I_{thr}	0.3 A	Δ_{min}	1.5°
	t	5		

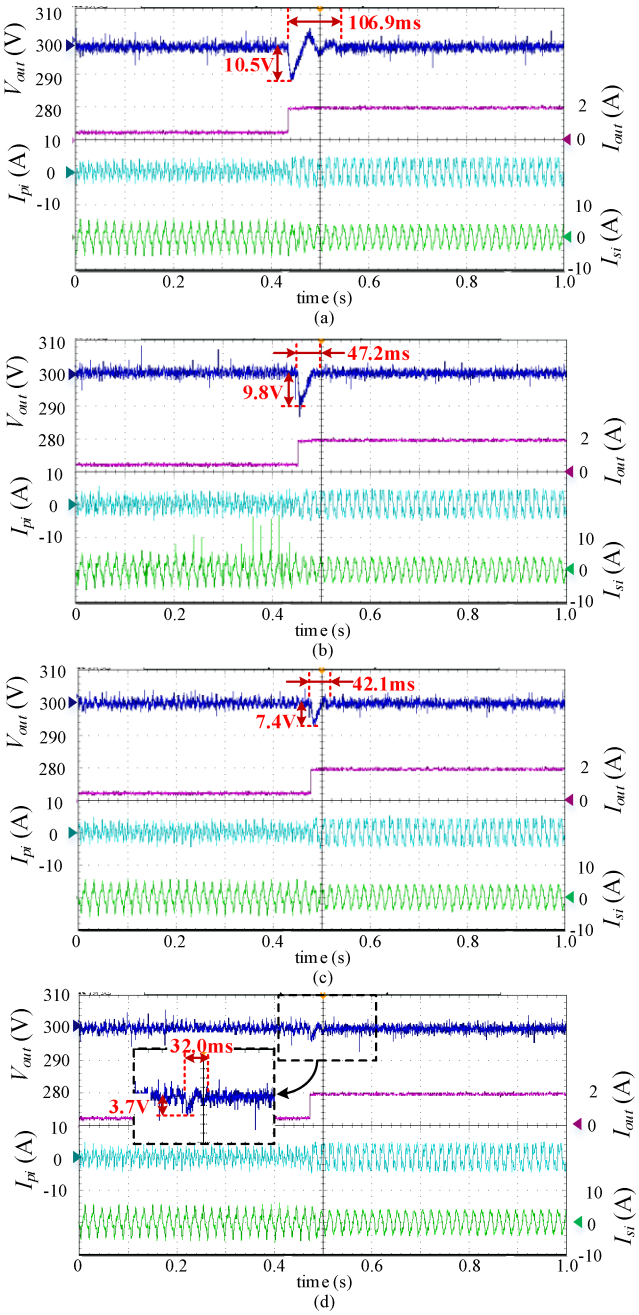

(a)

(b)

(c)

(d)

Fig. 17. Experimental results of different methods under the step load disturbance. (a) PI control. (b) FCS-MPC with constant step-size and $\alpha = 0$. (c) FCS-MPC with constant step-size and $\alpha = 4$. (d) FCS-MPC with adaptive step-size and $\alpha = 4$.

with the diameter of 0.1 mm. The air gap between the primary and secondary coils is set to 15 cm. The circuit parameters of the WPT system are given in Table III. The SiC power MOSFETs (SCH2080KE) are adopted as the semiconductor devices in dual-side converters, and ADuM3223 is adopted as the power MOSFET driver. TMS320F28335 DSP is utilized as microcontroller unit to implement the control algorithm, and the sampling frequency f_s is set to 20 kHz. The overall system efficiency is measured by the digital power meter (Yokogawa WT333E). The parameters of the proposed FCS-MPC and adaptive P&O methods are shown in Table IV.

B. Dynamic Response Verification of the Proposed FCS-MPC

To verify the effectiveness of the FCS-MPC method, the adaptive step-size and the improved cost function, the control performance comparison between PI control, FCS-MPC with constant step-size and $\alpha = 0$, FCS-MPC with constant step-size and $\alpha = 4$, and FCS-MPC with adaptive step-size and $\alpha = 4$ are shown in Fig. 17, where the voltage reference is 300 V and the load resistance steps from 600 to 150 Ω. As shown in Fig. 17(a) and (b), compared with the PI controller, the FCS-MPC without adaptive step-size and improved cost function is able to shorten the setting time with step load disturbance. However, there is still voltage overshoot of 9.8 V and the setting time is about 42.1 ms. As shown in Fig. 17(c), the introduction of improved cost function is able to enhance the dynamic response of FCS-MPC. The voltage overshoot is reduced to 7.4 V and the setting time is reduced to 42.1 ms. Eventually, as shown in Fig. 17(d), after adopting the proposed FCS-MPC that further introduces the adaptive step-size, the dynamic performance of the output voltage regulation is further improved. Compared with the FCS-MPC without adaptive step-size and improved cost function, the voltage overshoot is reduced by 62.2% and the setting time is reduced by 32.2%.

The performance comparisons between the PI controller and the FCS-MPC controller with the step load disturbance from 900 to 150 Ω are given in Figs. 18 and 19. As shown in Fig. 18, with the PI controller, the WPT system suffers from the voltage overshoot, oscillation, and long setting time. The voltage overshoot reaches about 13.5 V and the setting time is 140.2 ms. As shown in Fig. 19, after adopting the proposed FCS-MPC controller, the voltage overshoot is reduced to 4.4 V and the

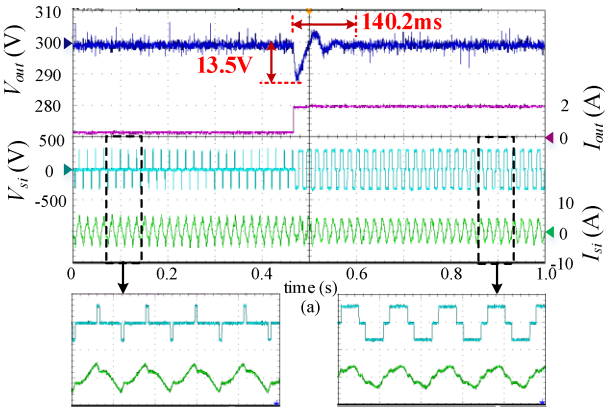

Fig. 18. Control performance of PI controller with the step load disturbance from 900 to 150 Ω.

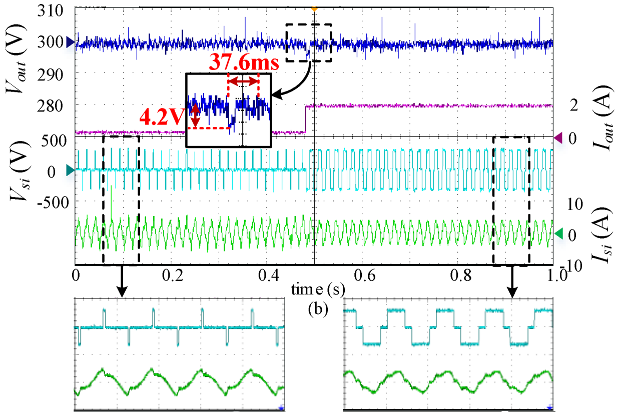

Fig. 19. Control performance of FCS-MPC controller with step load disturbance from 900 to 150 Ω.

setting time is reduced to 37.6 ms. It can be proved that the proposed FCS-MPC controller outperforms the PI controller in response to the step load disturbance. Moreover, the steady-state voltage and current waveforms of the secondary side converter in both methods are consistent, which confirms the steady-state efficacy of the proposed FCS-MPC.

The performance comparisons between PI control, FCS-MPC with constant step-size and $\alpha = 0$, FCS-MPC with constant step-size and $\alpha = 4$, and FCS-MPC with adaptive step-size and $\alpha = 4$ with step voltage reference variations are shown in Fig. 20, where the load resistance is 150 Ω. As seen from that with the PI controller, the system requires to take a long setting time to reach the voltage reference. The setting time is 108 and 152 ms with the voltage reference variation from 300 to 260 V and from 260 to 300 V, respectively. After adopting the FCS-MPC without adaptive step-size and improved cost function, the setting time is reduced to 51.2 and 112.2 ms, respectively. By introducing the improved cost function, the setting time can be further reduced to 44.2 and 105.6 ms, respectively. After adopting the proposed FCS-MPC controller, there is no noticeable voltage overshoot observed in the system output voltage. Meanwhile, the setting time can be reduced to 33 and 94 ms with the voltage reference variation from 300 to 260 V and from 260 to 300 V, respectively. The results confirm the superior performance of the proposed FCS-MPC controller in the regulation over the voltage reference.

Statistic comparisons of the PI control and FCS-MPC under different working conditions are described in Table V. It is obvious that FCS-MPC can provide the faster dynamic performance than PI control. The adaptive step-size and improved cost function also contribute to the reduction of the voltage overshoot and the setting time. Hence, the great dynamic performance of the proposed FCS-MPC can be verified.

Experimental results of the output voltage V_{out}, the output current I_{out} acquired by current sensor, the observed output current $\hat{I}_{out}$ ($\hat{I}_{out} = -z_2 \cdot C_f$), and the current I_{si} are shown in Fig. 21. The output current I_{out} is changed up from 0.5A to 1.67 A approximately as the load resistance is stepped up from 600 to 180 Ω. It is obvious that the observed output current by ESO is consistent with the actual current acquired by current sensor. Hence, it can be concluded that the extra current sensors can be avoided in the proposed FCS-MPC method, and the current sensorless control with fast response is achieved.

The execution time of single-step and two-stage series FCS-MPC with different n is evaluated as shown in Fig. 22. The PI controller takes 0.8 μs to implement, whereas the execution time of FCS-MPC varies with n. Because the two-stage series FCS-MPC only takes $(n + 3)/2$ number of rolling calculations to realize the same performance as the single-step FCS-MPC with n number of rolling calculations, experimental results show that for the case where the higher number of rolling calculations are needed, more execution time can be saved by adopting the two-stage series prediction scheme, compared to the single-step prediction scheme. $n = 11$ has already demonstrated the great performance against the PI controller. The execution time of single-step and two-stage series prediction scheme with $n = 11$ is 21.6 and 15.7 μs, respectively. The computational burden is reduced by 27.3% by adopting the proposed two-stage series FCS-MPC. Because 50 μs is available in one control period, there is sufficient time for implementing A/D sampling, system protections, digital filtering, etc. Although the computational burden of the improved FCS-MPC is still higher than that of PI control, it is acceptable for excellent dynamic performance. The execution time can be further reduced by using advanced controllers, such as the field-programmable gate array.

C. Efficiency Optimization Verification of Adaptive P&O Method

To verify the effectiveness of the proposed adaptive P&O method, experimental result comparisons about the search process of MEET between the conventional P&O method and the adaptive P&O method are shown in Fig. 23, where the load resistance is 600 Ω. Note that all of the experimental results presented below are based on the adoption of the proposed FCS-MPC method to regulate the output voltage. As seen from that without the MEET method, the dc input current of the WPT system is 0.63 A and the system efficiency is 79.4%. After adopting the conventional P&O method, the dc input current I_{in} can be decreased by perturbing the phase shift angle φ_p so as to track the maximum energy efficiency point. However,

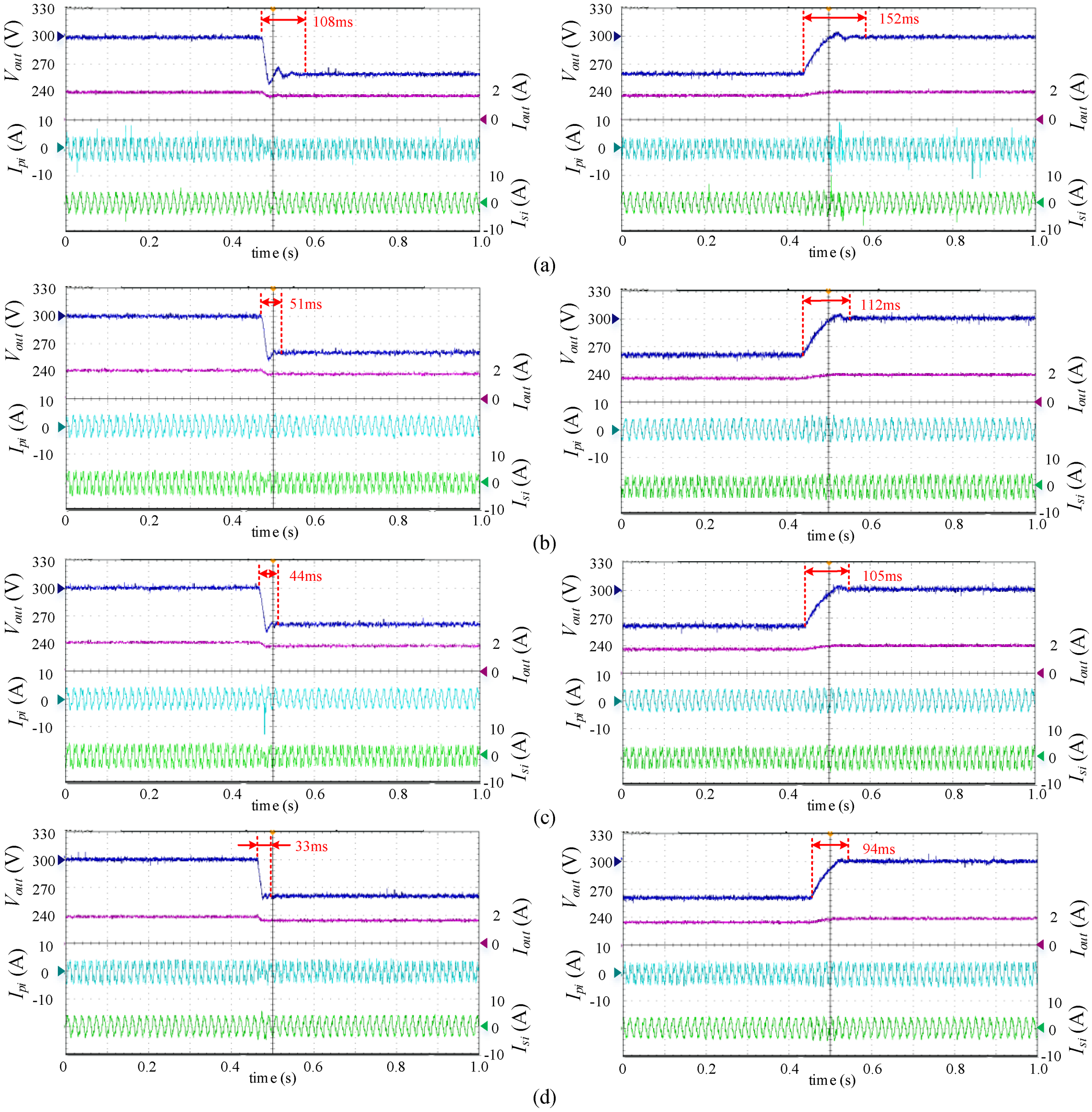

Fig. 20. Experimental results of different methods under the step voltage reference variation from 300 to 260 V and from 260 to 300 V. (a) PI control. (b) FCS-MPC with constant step-size and $\alpha = 0$. (c) FCS-MPC with constant step-size and $\alpha = 4$. (d) FCS-MPC with adaptive step-size and $\alpha = 4$.

TABLE V
CONTROL PERFORMANCE COMPARISON OF PI CONTROL AND FCS-MPC

	900 Ω→150 Ω		260 V→300 V		300 V→260 V	
	ΔV (V)	ΔT (ms)	ΔV (V)	ΔT (ms)	ΔV (V)	ΔT (ms)
PI control	10.5	106.9	6.9	152.0	12.3	108.0
FCS-MPC with Δf and $\alpha=0$	9.8	47.2	5.4	112.2	8.8	51.2
FCS-MPC with Δ_{adp} and $\alpha=0$	7.4	42.1	3.9	105.6	6.2	44.2
FCS-MPC with Δ_{adp} and $\alpha=4$	3.7	32.0	2.2	94.0	2.3	33.0

ΔV denotes the voltage overshoot and ΔT denotes the setting time.

after reaching the maximum efficiency point, the state of φ_p becomes a three-point oscillation stage as shown in Fig. 23, thus resulting in that the input system current fluctuates in the range of 0.56–0.60 A. This means that the system efficiency also varies in the range of 83.3%–89.3%, which is not conducive to the stability and efficiency optimization of the system. The system oscillation can be reduced by setting a small step-size, but the long tracking time for the maximum efficiency point is required. Hence, there is a tradeoff between the oscillation and the tracking time for the conventional P&O method. After

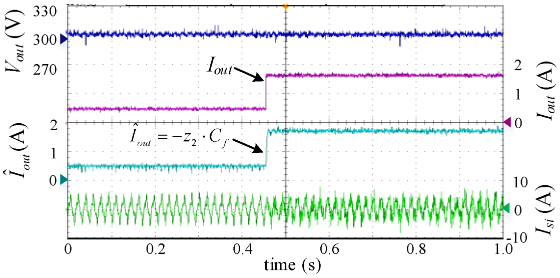

Fig. 21. Current observation result of ESO in FCS-MPC controller with step load disturbance.

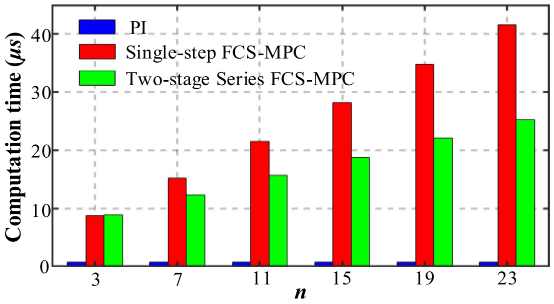

Fig. 22. Execution time comparison between PI control, single-step FCS-MPC, and two-stage series FCS-MPC.

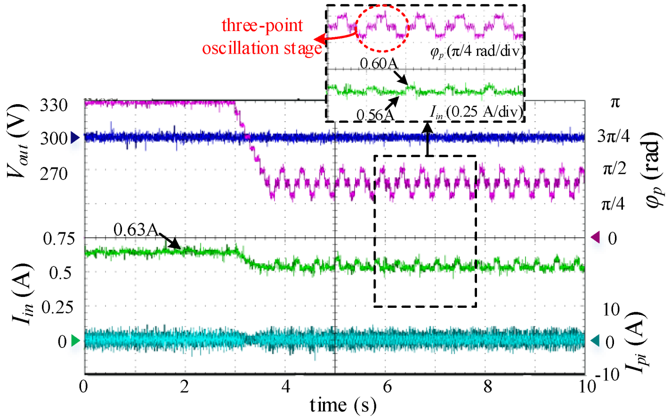

Fig. 23. Experimental results of search process of MEET with conventional P&O method.

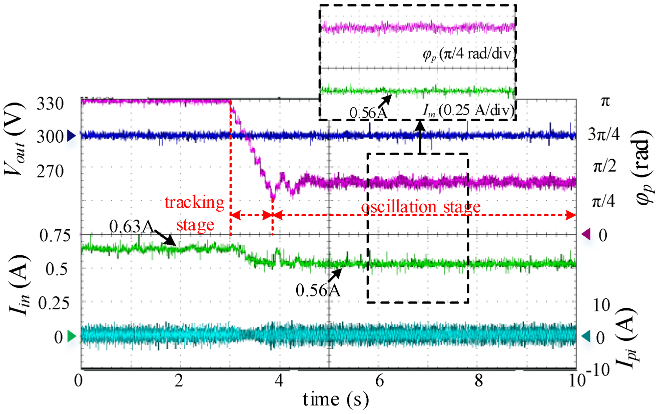

Fig. 24. Experimental results of search process of MEET with adaptive P&O method.

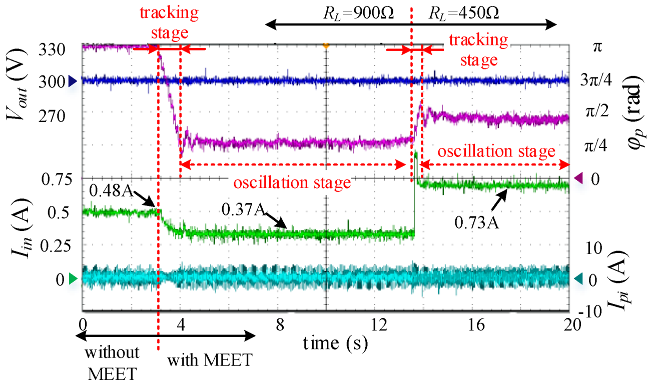

Fig. 25. Experimental verification of state switching conditions of adaptive P&O method.

utilizing the adaptive P&O method, as depicted in Fig. 24, the tracking stage and the oscillation state for the maximum efficiency point can be distinguished successfully, thereby providing the foundation for the implementation of the adaptive step-size. In the tracking stage, a large perturbation step-size of 15° is applied, which is consistent with the traditional P&O method. While the system enters the oscillation stage, the large perturbation step-size is continuously decreased by 1.5° in each control period until it reaches the small value of 1.5°. Then, the system state is locked in the oscillation stage with the step-size of 1.5° to avoid the unexpected state switching caused by a small external interference. Although there still exists the oscillation in the WPT system, this oscillation can be ignored due to the small value of perturbation step-size. The system input current can be maintained at 0.56 A and the system efficiency can be enhanced from 79.4% to 89.3%. It is proved that the adaptive P&O method is able to eliminate the tradeoff between the oscillation and the tracking time in the conventional method, and it is effective for the efficiency optimization.

To test the validity of the state switching conditions of adaptive P&O method, experimental results under the step load disturbance from 900 to 450 Ω with the proposed adaptive P&O method are shown in Fig. 25. As seen from that without the MEET method, the dc input current of the WPT system is 0.48 A and the system efficiency is 68.8%. After adopting the adaptive P&O method, the system enters the tracking state first, and the phase shift angle φ_p is continuously reduced by 15°. While the value of sum is reduced from 5 to less than 5, the system state is switched from the tracking stage to the oscillation state so that the system input current is reduced to 0.37 A and the system efficiency is enhanced to 89.2%. Then, the load resistance varies from 900 to 450 Ω, and the condition that $I_r \geq I_{thr}$ is satisfied. The system state can be successfully switched from the oscillation state to the tracking state for approaching the maximum efficiency point within the shortest time possible. Therefore, experimental results indicate that the design of state switching conditions in the adaptive P&O method is reasonable.

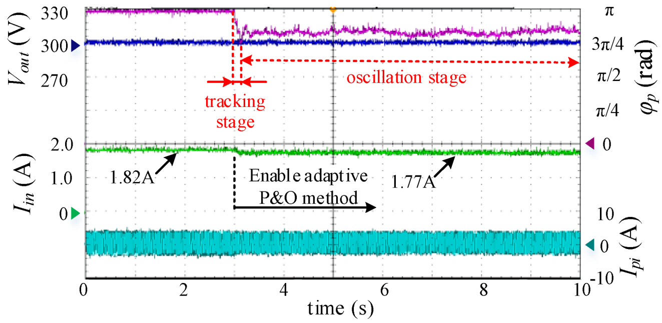

Fig. 26. Experimental verification of adaptive P&O method under the load of 180 Ω.

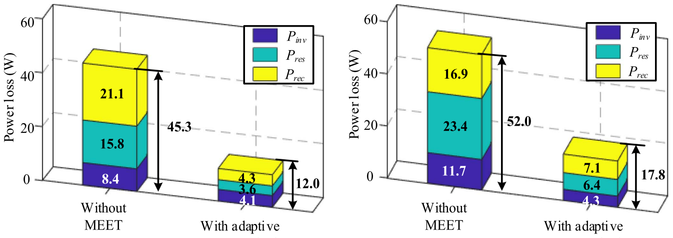

(a) (b)

Fig. 27. Power loss distributions of WPT system without MEET and with the adaptive P&O method. (a) When the output power is 100 W. (b) When the output power is 200 W.

The above experimental results demonstrate the effectiveness of the proposed algorithm under the light and medium load conditions. To further verify that the adaptive P&O method can operate effectively under the heavy conditions, experimental results of adaptive P&O method under the load of 180 Ω are shown in Fig. 26. After adopting the proposed algorithm, the tracking stage and the oscillation stage can still be successfully identified. The dc input current can be decreased from 1.82 to 1.77 A, and the corresponding φ_p is greater than that under the light load condition for the required output power. Hence, the effectiveness of adaptive P&O method under the heavy-load condition can be verified.

Power loss distributions of WPT system without MEET and with the adaptive P&O method when the output powers are 100 and 200 W are shown in Fig. 27. As seen from that the inverter loss P_{inv} and the rectifier loss P_{rec} are the nonnegligible part of the system power loss. While the output power is 100 W, the total power loss of WPT system without MEET is 45.3 W, including the inverter loss of 8.4 W, the resistance loss of 15.8 W, and the rectifier loss of 21.1 W. After adopting the adaptive P&O method, the inverter loss P_{inv}, the rectifier loss P_{rec}, and the resistance loss P_{res} can be reduced by 4.3 W (51.2%), 12.2 W (77.2%), and 16.8 W (79.6%), respectively. Furthermore, while the output power is 200 W, the inverter loss P_{inv}, the rectifier loss P_{rec}, and the resistance loss P_{res} can be reduced by 7.4 W (63.2%), 17.0 W (72.6%), and 9.8 W (58.0%), respectively. Hence, the effectiveness for efficiency improvement of the adaptive P&O method can be validated by experimental results.

The curves of the efficiency versus output power of the WPT system without MEET and with the adaptive P&O method are shown in Fig. 28. The system efficiency was calculated as the ratio of the output power to the input power with WT333E. As seen from that the system efficiency decreases with the reduction of output power. With a coupling coefficient k of 0.24 or 0.19, the system efficiency with the adaptive P&O method is significantly higher than that without MEET. While the output power is 600 W, the system efficiency after optimizing is able to reach 94.8%. Even under the light load condition, the system efficiency is above 89% and 85% for the coupling coefficient k of 0.24 and 0.19, respectively. Hence, the adaptive P&O method on the efficiency optimization can be verified.

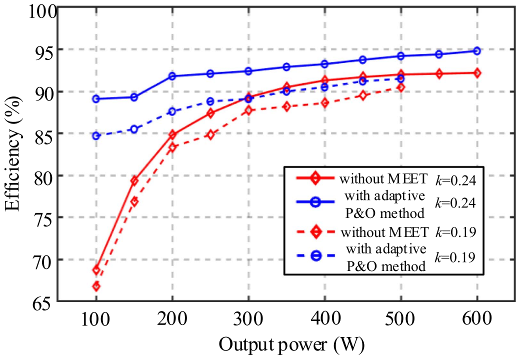

Fig. 28. Efficiency comparison of WPT system between without MEET and with the adaptive P&O method.

D. Comparison of the Reported and Proposed Methods

Some works about dynamic improvement or efficiency optimization of WPT systems have been reported in [16], [18], [23], [30], [36], [37], and [38]. It should be emphasized that the contributions of this article are to design the advanced control strategies for the dynamic improvement and efficiency optimization of WPT system. To clarify the innovation of this article, the summary and comparison of the reported and proposed methods are given in Table VI.

This work in [36] designs an H∞ controller for the fast response of *LCC–LCC* compensated WPT system without extra sensor and dc–dc converter. In [37], a feedforward control is proposed to enhance the dynamic capability of WPT system. However, an extra current sensor is required and a user-side dc–dc converter is also added, which leads to the increase of system cost and size. This work in [38] proposes a CCS-MPC method to realize the fast voltage regulation for dynamic WPT system. The extra current sensor and buck converter still cannot be avoided. Besides, for these methods in [36], [37], and [38], the work about efficiency improvement is not considered.

In [16], the formula calculation method is combined with a buck–boost converter for the CV output and efficiency optimization of WPT system. Similarly, the formula calculation method is also adopted in [18] to enhance the efficiency of S-S compensated WPT system. However, the formula calculation method ignores the losses of dual-side converters, and it depends on system parameters, which makes the maximum efficiency point difficult to track. Moreover, the PI control is utilized to

TABLE VI
SUMMARY AND COMPARISON OF THE REPORTED AND PROPOSED METHODS

References	Operating frequency	Dynamic response				Efficiency optimization		
		Method	Extra sensor	Extra dc–dc converter	Response speed	Method	Parametric dependence	Continuous perturbation
[16]	100 kHz	PI	No	Yes	Slow	Formula calculation	Yes	No
[18]	48 kHz	PI	No	No	Slow	Formula calculation	Yes	No
[36]	85 kHz	$H\infty$ control	No	No	Fast			
[37]	85 kHz	Feedforward control	Yes	Yes	Fast			
[38]	85 kHz	CCS-MPC	Yes	Yes	Fast			
[23]	100 kHz	SMC	No	No	Fast	P&O	No	Yes
[30]	80 kHz	FCS-MPC	Yes	No	Fast	P&O	No	Yes
This article	85 kHz	FCS-MPC	No	No	Fast	Adaptive P&O	No	Negligible

achieve the CV and current output, and there is still room for the improvement on dynamic response.

Both dynamic response and efficiency optimization are considered in [23] and [30]. This work in [23] designs an SMC controller for the dynamic improvement, which does not require the extra sensor and dc–dc converter. But the chattering problem of SMC is not discussed. The FCS-MPC is proposed in [30] for the extremely fast dynamic response, but two extra current sensors are needed and the computational burden is discussed. Both works adopt the P&O method to minimize the input power so as to maximize the system efficiency. Although this method is independent of system parameters, there is the continuous power perturbation exist in the WPT system. Compared to above methods, the improved FCS-MPC can avoid the use of extra sensors and relieve the computational burden to a certain extent, and the extra dc–dc converter is also unnecessary. Moreover, the adaptive P&O method can maintain the continuous perturbation that can be ignored without depending on system parameters, so that the maximum system efficiency reaches 94.8%.

VI. CONCLUSION

In this article, a novel FCS-MPC with the adaptive step-size and the improved cost function is designed for the stiff output voltage regulation of active rectifier of dual-side *LCL* compensated WPT systems. A linear ESO is introduced to incorporate FCS-MPC so as to avoid the extra current sensors, and the computational burden is relieved by designing a two-stage series prediction scheme. The rapid response of the system output can be achieved by the proposed FCS-MPC with relatively low computational burden and without current sensors. Then, on the premise of ensuring the stability of output voltage, an adaptive P&O method is proposed to achieve MEET by minimizing the input dc current. The tracking stage and the oscillation stage for MEET can be distinguished by recording the disturbance direction. The perturbation step-size adaptive to the system stage is designed to remove the tradeoff between the oscillation and the convergence rate existing in the conventional method. Finally, experimental comparisons of the proposed and conventional methods are carried out to verify the remarkable performance of the proposed FCS-MPC and P&O methods.

REFERENCES

[1] N. Tesla, “Apparatus for transmitting electrical energy,” U.S. Patent 1 119 732, Dec. 1, 1914.

[2] K. Li and W. Ding, “An improved one-to-three WPT system with tunable compensation network and enhanced pulse density voltage control,” *IEEE Trans. Emerg. Sel. Topics Power Electron.*, vol. 11, no. 3, pp. 3586–3596, Jun. 2023.

[3] A. A. S. Mohamed, A. Berzoy, F. G. N. De Almeida, and O. Mohammed, “Shielding design for high-frequency wireless power transfer system for EV charging with self-resonant coils,” *IEEE Trans. Power Electron.*, vol. 38, no. 6, pp. 7900–7909, Jun. 2023.

[4] Y. Jiang, L. Wang, J. Fang, C. Zhao, K. Wang, and Y. Wang, “A joint control with variable ZVS angles for dynamic efficiency optimization in wireless power transfer system,” *IEEE Trans. Power Electron.*, vol. 35, no. 10, pp. 11064–11081, Oct. 2020.

[5] N. Fu, J. Deng, Z. Wang, and D. Chen, “An LCC–LCC compensated WPT system with switch-controlled capacitor for improving efficiency at wide output voltages,” *IEEE Trans. Power Electron.*, vol. 38, no. 7, pp. 9183–9194, Jul. 2023.

[6] X. Tian, K. T. Chau, W. Liu, H. Pang, and C. H. T. Lee, “Maximum power tracking for magnetic field editing-based omnidirectional wireless power transfer,” *IEEE Trans. Power Electron.*, vol. 37, no. 10, pp. 12901–12912, Oct. 2022.

[7] Y. Liu, C. Liu, Z. Dong, S. Liu, and W. Wang, “A novel wireless energy router for home energy management with omnidirectional power transmission,” *IEEE Trans. Ind. Electron.*, vol. 70, no. 9, pp. 8979–8990, Sep. 2023.

[8] S. Pang, J. Xu, H. Li, Q. Ma, and X. Li, “Dual-frequency modulation to achieve power independent regulation for dual-load underwater wireless power connector,” *IEEE J. Emerg. Sel. Topics Power Electron.*, vol. 11, no. 2, pp. 2377–2389, Apr. 2023.

[9] W. Ding, K. Li, J. Yuan, J. Li, and C. Du, “Wireless power transmission-based in-wheel switched reluctance motor drive system with an x-type converter,” *IEEE Trans. Energy Convers.*, vol. 38, no. 1, pp. 450–462, Mar. 2023.

[10] K. Li, W. Ding, J. Yuan, and C. Du, “A decoupled multichannel based wireless SRM system with tunable compensation network and multifrequency pulse density control,” *IEEE Trans. Ind. Electron.*, to be published, doi: 10.1109/TIE.2023.3250748.

[11] J. H. Kim et al., “Development of 1-MW inductive power transfer system for a high-speed train,” *IEEE Trans. Ind. Electron.*, vol. 62, no. 10, pp. 6242–6250, Oct. 2015.

[12] S. Y. R. Hui, W. Zhong, and C. K. Lee, “A critical review on recent progress of mid-range wireless power transfer,” *IEEE Trans. Power Electron.*, vol. 29, no. 9, pp. 4500–4511, Sep. 2014.

[13] L. Xu, Q. Chen, X. Ren, S.-C. Wong, and C. K. Tse, “Self-oscillating resonant converter with contactless power transfer and integrated current sensing transformer,” *IEEE Trans. Power Electron.*, vol. 32, no. 6, pp. 4839–4851, Jun. 2017.

[14] J. Zhang, J. Zhao, Y. Zhang, and F. Deng, “A wireless power transfer system with dual switch-controlled capacitors for efficiency optimization,” *IEEE Trans. Power Electron.*, vol. 35, no. 6, pp. 6091–6101, Jun. 2020.

[15] Y. Li et al., “Extension of ZVS region of series–series WPT systems by an auxiliary variable inductor for improving efficiency,” *IEEE Trans. Power Electron.*, vol. 36, no. 7, pp. 7513–7525, Jul. 2021.

[16] X. Dai, X. Li, Y. Li, and A. P. Hu, “Maximum efficiency tracking for wireless power transfer systems with dynamic coupling coefficient estimation,” *IEEE Trans. Power Electron.*, vol. 33, no. 6, pp. 5005–5015, Jun. 2018.

[17] K. Song et al., “Constant current charging and maximum system efficiency tracking for wireless charging systems employing dual-side control,” *IEEE Trans. Ind. Appl.*, vol. 56, no. 1, pp. 622–634, Jan./Feb. 2020.

[18] B. X. Nguyen et al., “An efficiency optimization scheme for bidirectional inductive power transfer systems,” *IEEE Trans. Power Electron.*, vol. 30, no. 11, pp. 6310–6319, Nov. 2015.

[19] X. Zhang et al., “A control strategy for efficiency optimization and wide ZVS operation range in bidirectional inductive power transfer system,” *IEEE Trans. Ind. Electron.*, vol. 66, no. 8, pp. 5958–5969, Aug. 2019.

[20] Y. Liu, U. K. Madawala, R. Mai, and Z. He, “An optimal multivariable control strategy for inductive power transfer systems to improve efficiency,” *IEEE Trans. Power Electron.*, vol. 35, no. 9, pp. 8998–9010, Sep. 2020.

[21] S. Chen et al., “An operation mode selection method of dual-side bridge converters for efficiency optimization in inductive power transfer,” *IEEE Trans. Power Electron.*, vol. 35, no. 10, pp. 9992–9997, Oct. 2020.

[22] W. X. Zhong and S. Y. R. Hui, “Maximum energy efficiency tracking for wireless power transfer systems,” *IEEE Trans. Power Electron.*, vol. 30, no. 7, pp. 4025–4034, Jul. 2015.

[23] Y. Yang, W. Zhong, S. Kiratipongvoot, S.-C. Tan, and S. Y. R. Hui, “Dynamic improvement of series–series compensated wireless power transfer systems using discrete sliding mode control,” *IEEE Trans. Power Electron.*, vol. 33, no. 7, pp. 6351–6360, Jul. 2018.

[24] C. K. Hridya, R. Hari Kumar, and N. Mayadevi, “Wireless bidirectional power transfer with maximum efficiency point tracking control in electric vehicles,” in *Proc. IEEE Int. Conf. Power Electron., Smart Grid Renewable Energy*, Cochin, India, 2020, pp. 1–6.

[25] Y. Tang, Y. Chen, U. K. Madawala, D. J. Thrimawithana, and H. Ma, “A new controller for bidirectional wireless power transfer systems,” *IEEE Trans. Power Electron.*, vol. 33, no. 10, pp. 9076–9087, Oct. 2018.

[26] M. J. Neath, A. K. Swain, U. K. Madawala, and D. J. Thrimawithana, “An optimal PID controller for a bidirectional inductive power transfer system using multiobjective genetic algorithm,” *IEEE Trans. Power Electron.*, vol. 29, no. 3, pp. 1523–1531, Mar. 2014.

[27] J. Jiang, K. Song, Z. Li, C. Zhu, and Q. Zhang, “System modeling and switching control strategy of wireless power transfer system,” *IEEE J. Emerg. Sel. Topics Power Electron.*, vol. 6, no. 3, pp. 1295–1305, Sep. 2018.

[28] C. Qi, Z. Lang, L. Su, X. Chen, and H. Miao, “Model predictive control for a bidirectional wireless power transfer system with maximum efficiency point tracking,” in *Proc. IEEE Int. Symp. Predictive Control Elect. Drives Power Electron.*, 2019, pp. 1–5.

[29] C. Qi, Z. Lang, L. Su, X. Chen, and H. Miao, “Finite-control-set model predictive control for a wireless power transfer system,” in *Proc. IEEE Int. Symp. Predictive Control Elect. Drives Power Electron.*, 2019, pp. 1–5.

[30] S. Liu et al., “Dynamic improvement of inductive power transfer systems with maximum energy efficiency tracking using model predictive control: Analysis and experimental verification,” *IEEE Trans. Power Electron.*, vol. 35, no. 12, pp. 12752–12764, Dec. 2020.

[31] Y. Jiang, L. Wang, J. Fang, R. Li, R. Han, and Y. Wang, “A high-efficiency ZVS wireless power transfer system for electric vehicle charging with variable angle phase shift control,” *IEEE J. Emerg. Sel. Topics Power Electron.*, vol. 9, no. 2, pp. 2356–2372, Apr. 2021.

[32] Y. Li et al., “Efficiency analysis and optimization control for input-parallel output-series wireless power transfer systems,” *IEEE Trans. Power Electron.*, vol. 35, no. 1, pp. 1074–1085, Jan. 2020.

[33] S. Kouro, P. Cortes, R. Vargas, U. Ammann, and J. Rodriguez, “Model predictive control—A simple and powerful method to control power converters,” *IEEE Trans. Ind. Electron.*, vol. 56, no. 6, pp. 1826–1838, Jun. 2009.

[34] R. P. Aguilera, P. Lezana, and D. E. Quevedo, “Finite-control-set model predictive control with improved steady-state performance,” *IEEE Trans. Ind. Inform.*, vol. 9, no. 2, pp. 658–667, May 2013.

[35] T. Dragicevic and M. Novak, “Weighting factor design in model predictive control of power electronic converters: An artificial neural network approach,” *IEEE Trans. Ind. Electron.*, vol. 66, no. 11, pp. 8870–8880, Nov. 2019.

[36] Y. Liang et al., “H∞ robust control for ICPT system with selected weighting function considering parameter perturbations,” *IEEE Trans. Power Electron.*, vol. 35, no. 9, pp. 13914–13929, Nov. 2022.

[37] K. Chen, J. Pan, Y. Yang, and K. W. E. Cheng, “Stability improvement and overshoot damping of SS-compensated EV wireless charging systems with user-end buck converters,” *IEEE Trans. Veh. Technol.*, vol. 71, no. 8, pp. 8354–8366, Aug. 2022.

[38] Z. Zhou, L. Zhang, Z. Liu, Q. Chen, R. Long, and H. Su, “Model predictive control for the receiving-side DC–DC converter of dynamic wireless power transfer,” *IEEE Trans. Power Electron.*, vol. 35, no. 9, pp. 8985–8997, Sep. 2020.

Shuo Chen (Student Member, IEEE) was born in Shandong, China, in 1995. He received the B.S. degree in electrical engineering from Shandong University of Technology, Zibo, China, in 2017, and the M.S. degree in electrical engineering from China University of Mining and Technology, Xuzhou, China, in 2020. He is currently working toward the Ph.D. degree in electrical engineering with Xi’an Jiaotong University, Xi’an, China.

His research interests include the wireless power transfer and drive control of permanent magnet synchronous motors.

Wen Ding (Member, IEEE) received the M.S. and Ph.D. degrees in electrical engineering from Xi’an Jiaotong University, Xi’an, China, in 2006 and 2009, respectively.

He is currently an Associate Professor with the School of Electrical Engineering, Xi’an Jiaotong University. His research interests include electrical machines and drives with emphasis on permanent magnet synchronous machines and reluctance machines, energy conversion systems, power electronics, electric vehicles, and wireless power transmission.

Lujie Huo (Student Member, IEEE) received the B.S. degree in electrical engineering from China University of Mining and Technology, Xuzhou, China, in 2022. He is currently working toward the M.S. degree in electrical engineering with the School of Electrical Engineering, Xi’an Jiaotong University, Xi’an, China.

His research interests include the reduced dc-link capacitance permanent magnet synchronous motor drives and the sensorless control of permanent magnet synchronous motor.

Xiang Wu (Member, IEEE) was born in Jiangsu, China, in 1990. He received the B.S. and Ph.D. degrees in electrical engineering and automation from China University of Mining and Technology, Xuzhou, China, in 2013 and 2019, respectively.

He is currently a Lecturer of power electronics and electrical drives with the School of Electrical and Power Engineering, China University of Mining and Technology. His research interests include power electronics, modern control theory, battery management systems, and motor.

Shuai Shi received the B.S. degree in electrical engineering from Zhengzhou University, Zhengzhou, China, in 2020. He is currently working toward the M.S. degree in electrical engineering with the School of Electrical Engineering, Xi’an Jiaotong University, Xi’an, China.

His research interests include the design of wireless power transfer and drive control of permanent magnet synchronous motors.

Ruiming Hu received the B.S. degree in electrical engineering from Taiyuan University of Technology, Taiyuan, China, in 2020. He is currently working toward the master’s degree in electrical engineering with the School of Electrical Engineering, Xi’an Jiaotong University, Xi’an, China.

His current research focuses on the design and drive control of permanent magnet assisted synchronous reluctance motors.